Simulation of 1D SSH model in Electrical Circuits

A laboratory project report to be submitted by

Jabed Umar, Dikkar Shubhay

Roll. No - 2011072, 2011059

School of Physical Sciences

National Institute of Science Education and Research

Jatni, Khurda, Bhubaneswar, 752050, India

Under the supervision of

Dr. Kartikeswar Senapathi, Dr. Saralasita Mohanty

August - November 2023

Abstract

Topology, a mathematical concept investigating properties of geometric objects invariant under continuous deformations, has found practical realization in a physical system after the groundbreaking discovery of the quantum Hall effect, illuminating topological phases of matter. This project explores a novel method to induce topological phases of matter in an LC circuit, guided by its circuit Laplacian, analogous to the Hamiltonian in tight-binding lattice models. The focus is on simulating the Su-Schrieffer–Heeger (SSH) model, a tangible platform demonstrating the practical realization of topological phenomena, where robust zero-energy topological boundary modes emerge prominently with a significant boundary impedance tuned to the resonance frequency through an analytical understanding, simulation techniques and experimental investigations of the impedance profile.

Contents

1 Introduction 3
2 Aim of the Project 4
3 Methodology 5
3.1 Chapter 1: Electrical Circuits and Graphs 5
Nodal Analysis of Electrical Circuits 5
Impedance Between Any Arbitrary Points 8
3.2 Chapter 2: SSH Model and its Circuit Represenation 10
1D SSH Model 10
Electrical Circuit Representation of SSH Model 15
3.3 Chapter 3: Study of Simulated Circuit 19
Simulation using Python 19
Simulation using LT spice 22
3.4 Chapter 4: Experimental Implementation 25
Brief on Lock In Amplifier 25
Impedance Profile 26
4 Result and Analysis 28
5 Conclusion 29
6 Future Plans 30
7 References 32

1 Introduction

The mathematical concept of topology, which plays a central role in this work, is a field that deals with the properties of geometric objects. These properties remain invariant under continuous deformations and are independent of the specific shape of the objects. This concept forms the foundation for understanding the topological aspects encountered in this research.

A pivotal moment in developing topological physics was the discovery of the quantum Hall effect [7] by Klaus von Klitzing in 1980. This groundbreaking discovery revealed the quantization of the Hall resistance in a two-dimensional electron gas exposed to a magnetic field. The profound aspect of this phenomenon was that it could be explained by topological invariants, leading to the concept of topological phases of matter.

This work explores the intriguing parallels between topological concepts in solid-state physics and electric circuit networks (chapter 1 and 2), which serve as our chosen platform. Electric circuits offer distinct advantages, while these parallels might not be as immediately apparent as in other quantum mechanical systems or systems described by Schrödinger equations. These advantages include accessibility, tunability, well-established manufacturing processes, and various commercially available circuit components. This makes electric circuits a powerful tool for experimentally investigating the impact of topology on translation-invariant lattices.

Our project journey begins with the experimental exploration of Hermitian circuits, allowing us to establish general design principles for topolectrical circuits. Subsequently, we investigate topological edge modes within the SSH model, as detailed in chapter 3 and 4. Through computer simulations and experiments conducted on LC circuits, we gain insights into the topological behaviour of the circuit and how it fundamentally differs from the trivial phase.

In essence, this work represents a unique fusion of mathematical topology, condensed matter physics, and electrical circuitry, offering an experimental lens through which we can explore and understand the intriguing world of topological physics.

2 Aim of the Project

Firstly, the project aims to comprehensively understand the Laplacian formalism and subsequently establish its connection with a tight-binding Hamiltonian through circuit analysis. This endeavour holds immense importance as it allows us to study a tight-binding model, a fundamental and indispensable topic in condensed matter physics. Through circuit analysis, we aim to bridge the conceptual gap between these seemingly distinct domains, thereby gaining a unique perspective on the intricate relationships within quantum physics.

Secondly, the project investigates a tight-binding model, specifically one with two distinct hopping amplitudes known as the SSH model, within the context of an electrical circuit. The SSH model is a crucial starting point in the fascinating field of Topological physics. By conducting experiments with this model, we aim to validate and explore the topological properties inherent to such systems. This aspect of the project enables us to deepen our understanding of topological phases and offers a tangible means of verifying these properties within the confines of an electrical circuit.

3 Methodology

3.1 Chapter 1: Electrical Circuits and Graphs

Nodal Analysis of Electrical Circuits

Our experiment uses a 'Lumped Electrical Model' to analyze the circuit, treating components like resistors, capacitors, and inductors as concentrated points. This simplification lets us focus on nodal points, and by using Kirchoff's law (KCL & KVL), we can find out the flow of currents (I) and voltages (V) between them. However, deriving these relationships can be daunting for large and complex circuits. To overcome this, we employ the Laplacian Formulation, introduced by C. Lee et al.[5] offers a systematic approach for simplifying the analysis of intricate circuits, making it more efficient and manageable.

To analyze complex electrical networks, we will use a common tool in electrical engineering called nodal analysis, where any electrical circuit network can be represented by a graph whose nodes and edges correspond to the circuit junctions and connecting wires/elements. Let us start by taking a simple example that can no longer be solved by series and parallel circuits and has to be solved with nodal analysis.[6]

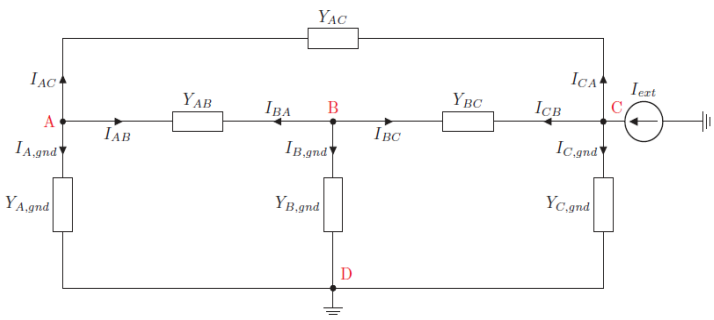

Figure 1: **A four-node (red) electrical circuit network with node D as ground, and node C connected to an external current source, comprising six circuit elements characterized by their admittances Y.**[6]

By applying KCL, we will get the following equations,

$$I_{A,gnd} + I_{AB} + I_{AC} = 0 \tag{1}$$

$$I_{BA} + I_{B,gnd} + I_{BC} = 0 \tag{2}$$

$$I_{CA} + I_{CB} + I_{C,gnd} = I_{ext} \tag{3}$$

The internal currents are expressed in terms of node voltages and admittances between

the nodes.

$$Y_{A,gnd}.V_A + Y_{AB}.(V_A - V_B) + Y_{AC}.(V_A - V_C) = 0 \tag{4}$$

$$Y_{AB}.(V_B - V_A) + Y_{B,gnd}.V_B + Y_{BC}.(V_B - V_C) = 0 \tag{5}$$

$$Y_{AC}.(V_C - V_A) + Y_{BC}.(V_C - V_B) + Y_{C,gnd}.V_C = I_{ext} \tag{6}$$

This all can be represented in the matrix,

$$\begin{pmatrix} 0 \\ 0 \\ I_{ext} \end{pmatrix} = \begin{pmatrix} Y_{A,gnd} + Y_{AB} + Y_{AC} & -Y_{AB} & -Y_{AC} \\ -Y_{AB} & Y_{B,gnd} + Y_{AB} + Y_{BC} & -Y_{BC} \\ -Y_{AC} & -Y_{BC} & Y_{C,gnd} + Y_{AC} + Y_{BC} \end{pmatrix} \begin{pmatrix} V_A \\ V_B \\ V_C \end{pmatrix}$$

$$\implies \quad I = J \cdot V \tag{7}$$

Where J is known as the Laplacian of the circuit. We can Calculate the nodal Voltages by inverting the (J), and then the current is calculated by using the above equation,

$$I_{AB} = Y_{AB} \cdot (V_A - V_B) \tag{8}$$

To see the relation between the Laplacian of the circuit (J) with the continuum Laplacian (∇^2), consider the spreading of current from a single node as a divergence of current density $I = -\nabla \cdot j$ and invoke the definition of conductivity $j = \sigma E = \sigma \nabla V$. Hence, for the current and voltage vectors as in equation-7, $I = \nabla \cdot (\sigma \nabla V) = \sigma \nabla^2 V = JV$. This establishes L as the continuum Laplacian restricted to a circuit.

Let us construct the circuit's Laplacian using graph theory without using the KCL and KVL. The graph is an ordered pair of two sets: a set of vertices 'V' and a set of Edge 'E'. We can represent the graph in a matrix form by defining the Adjacency Matrix (C), Which depicts the connection of nodes, and the Degree matrix (D), which gives information about the edges connecting different Nodes. The degree of a node is defined as the number of edges coming out of it.

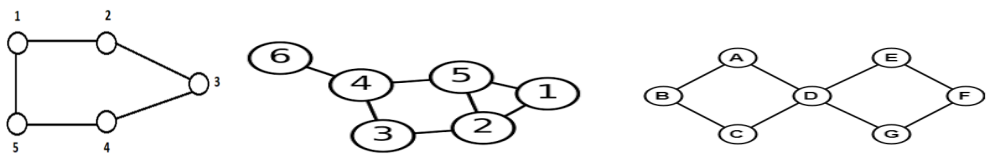

Figure 2: **Examples of Graphs, here circles are nodes and connecting lines are edges of the graph**

The Adjacency matrix (C) is a binary matrix where a value of 1 is assigned to a Matrix element C_{ij} if i^{th} Node is connected to j_{th} Node and Value 0 is assigned if they are not connected. The Degree matrix (D) is defined as follows:

$$D_{ij} = \begin{cases} deg(v_i), & \text{if } i = j \\ 0, & \text{otherwise} \end{cases} \tag{9}$$

Thus, the Adjacency (C) and Degree matrix (D) of the first graph in the above figure will be the following:

$$C = \begin{pmatrix} 0 & 1 & 0 & 0 & 1 \\ 1 & 0 & 1 & 0 & 0 \\ 0 & 1 & 0 & 1 & 0 \\ 0 & 0 & 1 & 0 & 1 \\ 1 & 0 & 0 & 1 & 0 \end{pmatrix} \quad and \quad D = \begin{pmatrix} 2 & 0 & 0 & 0 & 0 \\ 0 & 2 & 0 & 0 & 0 \\ 0 & 0 & 2 & 0 & 0 \\ 0 & 0 & 0 & 2 & 0 \\ 0 & 0 & 0 & 0 & 2 \end{pmatrix} = diag(\sum_i C_{1i}, \sum_i C_{2i}, ..) \tag{10}$$

And the Laplacian matrix of the graph is defined as L = D - C.

But in circuit theory, some circuit nodes can connect to the ground. So, to complete the conductance matrix, we need the notion of Grounded Laplacian (J) defined as J = L + W, where W is the grounded circuit matrix with diagonal entries of admittances connecting to the ground.

Let us now write down the Grounded Laplacian from the graph theory of the given circuit (see Figure 1) and check its consistency. The graph of the circuit[1] will be as follows.

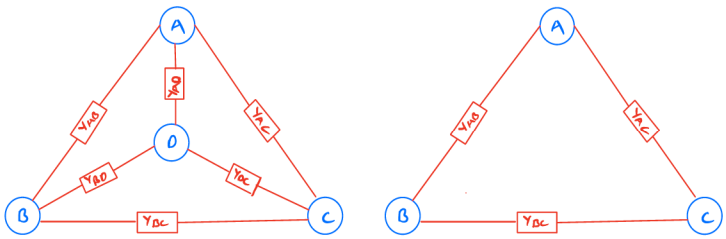

Figure 3: **Graph of the Circuit (Grounded and without Grounded Nodes)[1]**

The corresponding Adjacency matrix (C), Degree matrix (D) and Ground Matrix (W) will be as follows

$$C = \begin{pmatrix} 0 & Y_{AB} & Y_{AC} \\ Y_{AB} & 0 & Y_{BC} \\ Y_{AC} & Y_{BC} & 0 \end{pmatrix}, \quad D = \begin{pmatrix} Y_{AB} + Y_{AC} & 0 & 0 \\ 0 & Y_{AB} + Y_{BC} & 0 \\ 0 & 0 & Y_{AC} + Y_{BC} \end{pmatrix} \quad and$$

$$W = \begin{pmatrix} Y_{A,gnd} & 0 & 0 \\ 0 & Y_{B,gnd} & 0 \\ 0 & 0 & Y_{C,gnd} \end{pmatrix}$$

Thus, We confirm that J = (D - C + W) is the same as the matrix obtained in the nodal analysis.

$$\begin{pmatrix} Y_{A,gnd} + Y_{AB} + Y_{AC} & -Y_{AB} & -Y_{AC} \\ -Y_{AB} & Y_{B,gnd} + Y_{AB} + Y_{BC} & -Y_{BC} \\ -Y_{AC} & -Y_{BC} & Y_{C,gnd} + Y_{AC} + Y_{BC} \end{pmatrix}$$

Impedance Between Any Arbitrary Points

A central problem in electric circuit theory studied by many people over many years is the computation of the resistance between two nodes in a resistor network. Kirchhoff formulated the study of electric networks more than 150 years ago as a linear analysis. Let the electric potential at the i_{th} node by V_i and the net current flowing into the network at the i_{th} node by I_i. The Kirchhoff law states,

$$\sum_{j=1, j\neq i}^{N} c_{ij}(V_i - V_j) = I_i \implies LV = I \implies V = GI \implies V_i = \sum_{j=1, j\neq i}^{N} G_{ij} I_j \tag{11}$$

L is known as the Laplacian or Kirchhoff matrix, and the inverse of L is known as Green's function (G) of the circuit.

Resistance $R_{\alpha\beta}$ between two nodes α and β can be computed by knowing the potentials at the two nodes and the current passing through the nodes. Let the voltage at those nodes be V_α, V_β and the current passing through the node is I. Then, by Ohm's law, the desired resistance is

$$R_{\alpha\beta} = \frac{V_\alpha - V_\beta}{I} \tag{12}$$

The matrix element L_{ij} denote the conductance (or admittance) between i and j nodes, and since $L_{ij} = L^*_{ji}$. Therefore, L is a Hermitian matrix ($L = L^\dagger$). So, the eigenvalues of L will be real, and the eigenvectors will be orthogonal and complete.

Let's consider a resistance network whose Laplacian (L) has non-zero eigenvalues λ_i with orthonormal eigenvectors $\psi_i = (\psi_{i1}, \psi_{i2}, ..., \psi_{iN})$, i = 2, 3,..., N. Then the resistance between nodes α and β is

$$R_{\alpha\beta} = \sum_{i=2}^{N} \frac{|\psi_{i\alpha} - \psi_{i\beta}|^2}{\lambda_i} \tag{13}$$

Proof : The L matrix has a zero eigenvalue, so L^{-1} does not exist. To avoid this issue, add a small term ϵI to the Laplacian, where I is the N $\times$ N identity matrix and $\epsilon \to 0$. The modified Laplacian $L(\epsilon) = L + \epsilon I$ is the same form as L, except that the diagonal elements c_i are replaced by $c_i + \epsilon$. It is clear that $L(\epsilon)$ has eigenvalues $\lambda_i + \epsilon$ and is diagonalized by the same unitary transformation which diagonalizes L.

The inverse of $L(\epsilon)$, the Green's function, is now well defined, and we write $G(\epsilon) = L^{-1}(\epsilon)$. Let U be the unitary matrix which diagonalizes $L(\epsilon)$ and L, namely, $U^\dagger L U = \Lambda$ and $U^\dagger L(\epsilon) U = \Lambda(\epsilon)$. The elements of U are $U_{ij} = \psi_{ji}$, and Λ and $\Lambda(\epsilon)$ are, respectively, diagonal matrices with elements $\lambda_i \delta_{ij}$ and $(\lambda_i + \epsilon)\delta_{ij}$. From the Green's function equation,

$$U^\dagger G(\epsilon) U = \Lambda^{-1}(\epsilon) \implies G(\epsilon) = U \Lambda^{-1}(\epsilon) U^\dagger$$

or, explicitly,

$$G_{\alpha\beta}(\epsilon) = \sum_{i=1}^{N} U_{\alpha i} \frac{1}{(\lambda_i + \epsilon)} U^*_{\beta i} = \frac{1}{N\epsilon} + \sum_{i=2}^{N} \frac{\psi_{i\alpha}\psi^*_{i\beta}}{(\lambda_i + \epsilon)} = \frac{1}{N\epsilon} + g_{\alpha\beta} \tag{14}$$

(Since the sum of all columns (or rows) of L is identically zero, one of the eigenvalues of L is zero. It is readily verified that the zero eigenvalue $\lambda_1 = 0$ has the eigenvector $\psi_{1\alpha} = \frac{1}{\sqrt{N}}$, $\alpha = 1, 2, \ldots, N$.)[1]

By using the equation 4, 1 and $\sum_{j=1}^{N} I_j = 0$, we can write

$$V_i = \sum_{j=1, j\neq i}^{N} g_{ij}(\epsilon) I_j = \sum_{j=1, j\neq i}^{N} g_{ij}(0) I_j \tag{15}$$

If the current at i_{th} node is of the form $I_i = I(\delta_{i\alpha} - \delta_{i\beta})$ then by equation 2 and 5

$$R_{\alpha\beta} = \sum_{j=1}^{N} (g_{\alpha j} - g_{\beta j})(\delta_{j\alpha} - \delta_{j\beta}) = g_{\alpha\alpha} - g_{\beta\alpha} - g_{\alpha\beta} + g_{\beta\beta} \tag{16}$$

By putting the g_{ij} in terms of ψ_{ij} , we will get $R_{\alpha\beta} = \sum_{i=2}^{N} \frac{|\psi_{i\alpha} - \psi_{i\beta}|^2}{\lambda_i}$. (Proved)

The important point of the above discussion is that whenever the Laplacian (L) contains zero eigenvalues, that eigenmode will not contribute to the resistance between any two circuit nodes.

3.2 Chapter 2: SSH Model and its Circuit Represenation

1D SSH Model

The Su-Schrieffer-Heeger (SSH) model is a tight binding model that describes a single spin-less electron on a two-site unit cell 1D lattice. The two sites in a unit cell are labelled as A and B. It was first investigated by W.P. Su, J.R. Schrieffer and A.J. Heeger during their research on solitons in polyacetylene[3].

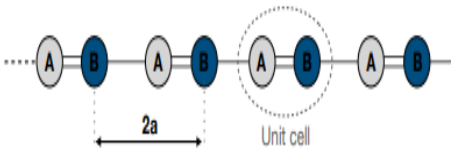

Figure 4: **Visual Representation of SSH Model**[2]

We will work with one electron per unit cell corresponding to a half-filled lattice because we consider spin-less electrons. Thus, the only degree of freedom the electrons have is that they can hop from one site to another. Let us consider v (for hopping within the unit cell) and w (for hopping connecting neighbouring unit cells), and write the bulk Hamiltonian (or far from the boundary) as

$$H = \sum_x [v(c^\dagger_{x,A} c_{x,B} + h.c) + w(c^\dagger_{x,B} c_{x+1,A} + h.c)] \tag{17}$$

Here, 'h.c.' denotes the hermitian conjugate of the term before it. Since it is a periodic system, we can go to the Fourier space ($c_x = \frac{\sum_k e^{-ikx} c_k}{\sqrt{N}}$) and write the Hamiltonian regarding creation ($c^\dagger_k$) and annihilation (c_k) operators in momentum space.

$$H = \sum_k c^\dagger_k M(k) c_k \tag{18}$$

Where,

$$M(k) = \begin{pmatrix} 0 & v + we^{ik} \\ v + we^{-ik} & 0 \end{pmatrix}$$

Now, upon diagonalizing this two-dimensional matrix, we can get the bulk dispersion relation in terms of the energy eigenvalues :

$$E(k) = \pm\sqrt{v^2 + w^2 + 2vw\cos k} \tag{19}$$

And the eigenvectors are of the form $\begin{pmatrix} \pm e^{-i\phi(k)} \\ 1 \end{pmatrix}$ where $\phi(k) = \tan^{-1} \frac{-w \sin k}{(v + w \cos k)}$.

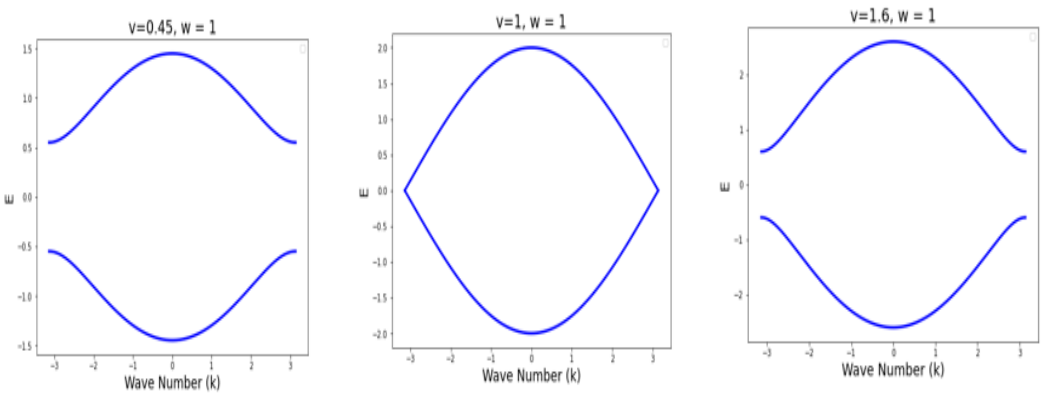

Figure 5: **Dispersion relation of bulk Hamiltonian for different v and w = 1**

The above figure shows that different choices of v and w will lead to different dispersion relations. Here we have considered the Fermi energy to be the zero energy level (this is the origin in our energy scale relative to which all other energies are measured here). The plots in the figure suggest that when v$\neq w$ (staggering case), in the Hamiltonian, the dispersion is gapped; hence, a staggered case would be an insulator. But for v = w, the gap closes, and there are states available above the Fermi level; therefore, the v = w case is a metal.

From the Bulk Hamiltonian, it seems like the problem is symmetric about the v = w case, or the v > w case is the same as the v < w case. But this is not quite right. The information obtained from the 'eigenvalues' is not complete! We need to also look at the eigenvectors to get complete information. And interestingly, the topological aspect is hidden in the eigenvectors.

To visualize the eigenvectors let us write M(k) in Pauli matrix (σ_i) basis or

$$M = d(k) \cdot \sigma = \begin{pmatrix} v + w \cos k & -w \sin k & 0 \end{pmatrix} \begin{pmatrix} \sigma_x \\ \sigma_y \\ \sigma_z \end{pmatrix} \tag{20}$$

By comparing with the eigenvectors we will get $\phi(k) = \tan^{-1} \frac{d_y(k)}{d_x(k)}$. Therefore, in the d_x-d_y space, the direction of the vector d(k) denotes an eigenstate, and the magnitude of the vector will give its eigenvalue. If we plot the trajectories for the two seemingly equivalent cases (v >w and v <w), we observe (see figure below) that even though their dispersions

(see E vs k graph) are similar, these trajectories on the d_x-d_y plane are very different! For one of the insulating cases (v <w), the vector d(k) winds about the origin, and for the other case (v >w), it does not.

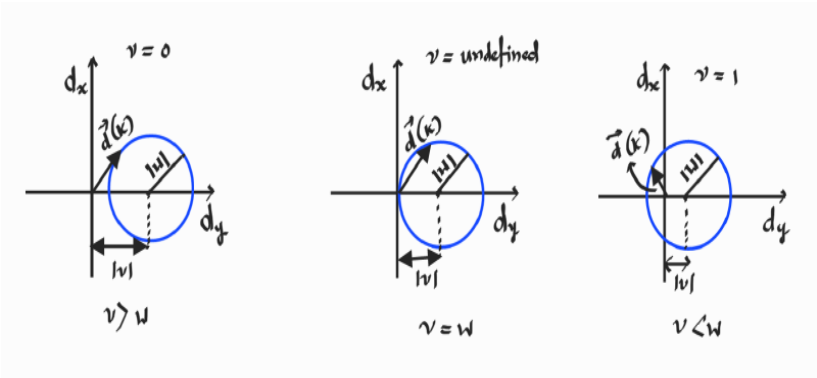

Figure 6: **Trajectories of d(k) in d_x-d_y plane**

The winding number (ν), related to Berry's potential [2], is the topological invariant quantity [2] that tells us whether the trajectory of d(k) winds about the origin or not. This disguises the two seemingly same cases and is defined as [4],

$$\nu = \frac{1}{2\pi}\int_{-\pi}^{\pi}\left(n(k)\times\frac{d}{dk}n(k)\right)_z dk \;=\begin{cases} 0,\ (trivial) & \text{if } v>w \\ 1,\ (topological) & \text{if } v<w \\ undefined, & \text{if } v=w \end{cases} \tag{21}$$

Where n(k) = $\frac{d(k)}{|d(k)|}$, is the normalised eigenvector. And ν is undefined for the v = w case since the notion of the filled band itself is undefined.

In the real system, we consider a finite SSH chain with open boundaries instead of the infinitely long chain with periodic boundary conditions previously discussed. This problem is not trivial; since there is no translational invariance, we can't use the Fourier transformation to diagonalize the Hamiltonian. The Hamiltonian of the system will be

$$H = \sum_{x=1}^{N}[v(c^{\dagger}_{x,A}c_{x,B} + h.c) + w(c^{\dagger}_{x,B}c_{x+1,A} + h.c)] = C^{\dagger}AC \tag{22}$$

Where A is 2N×2N tridiagonal matrix, known as the SSH matrix for finite chain and of

the form,

$$A = \begin{pmatrix} 0 & v & 0 & 0 & .. \\ v & 0 & w & 0 & ... \\ 0 & w & 0 & v & .. \\ 0 & 0 & v & 0 & w.. \\ 0 & 0 & 0 & .... & 0 \end{pmatrix}_{2N\times 2N} \quad and \quad C = \begin{pmatrix} c_{1A} \\ c_{1B} \\ c_{2A} \\ c_{2B} \\ ... \end{pmatrix}_{2N\times 1}$$

Let us first analyze the behaviour in the extreme case or dimerized limit (w = 0, v $\neq$0 and v = 0, w $\neq$0).

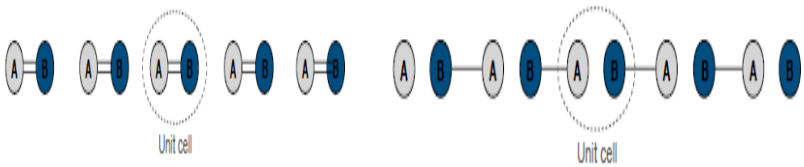

Figure 7: **Finite SSH chain in the limit w = 0 and v = 0**[2]

The w = 0 case corresponds to a dimerized chain, which is relatively straightforward. In this case, the solution can be represented as the superposition of the A and B sites within each dimer unit. This configuration aligns with the expectation of an insulating state because the chain is effectively broken, preventing particles from hopping between the ends due to the absence of connections between dimers.

Now, for the v = 0 case, we also get a few dimers, but since the chain has open boundaries, we now have two single sites at the end of the chain (see above figure). In the SSH model, the absence of energy contribution for an electron fixed at one site implies a zero energy contribution for those two electrons in this context. Therefore, we should expect two zero energy states in the system localized at the edges of the chain. And, by a similar argument, we also expect this case to be an insulator.

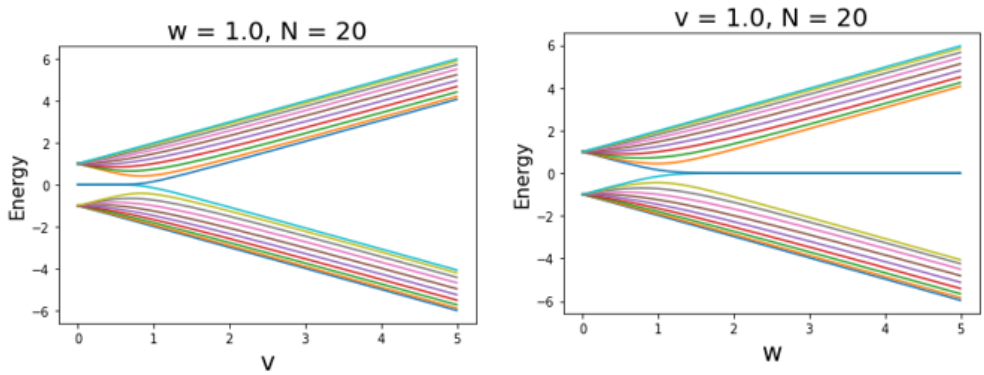

Figure 8: **Eigenvalue spectrum as a function of v and w**[2]

The Hamiltonian for an open SSH chain can be solved exactly through numerical methods. As depicted in the figure above, the eigenspectrum closely aligns with the anticipated results, depending on the parameters v and w [2]. For the dimerized case, we indeed see zero energy states (very close to zero) in the case where v = 0 and no zero energy states w = 0 case. Interestingly, the zero energy states also exist for non-zero v. Nonetheless, there is some uncertainty regarding its insulating behaviour because of zero energy states in the case of v = 0. However, intuitively, a dimerized chain is not expected to conduct, and the zero energy states should be localized at the boundary.

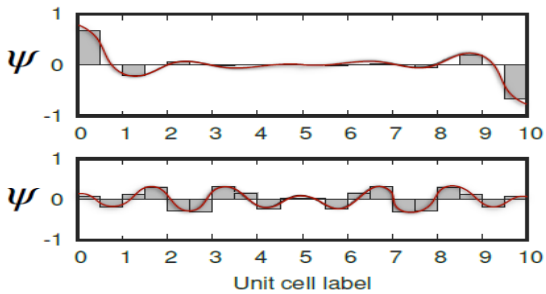

Figure 9: **Wavefunction amplitude at each site corresponding to zero energy edge states and non-zero energy eigenstate.**[2]

The Examination of the wavefunctions (see figure above) corresponding to the energy eigenstates reveals that the non-zero energy state exhibits delocalization across the entire chain. Conversely, the zero energy states, considered edge states, exhibit exponential localization at the chain's edges with localization length $\ln\left(\frac{v}{w}\right)$, consistent with the dimerized limit expectation. It's worth noting that these zero energy edge states persist only when v < w; if v > w, these states become non-normalizable and unphysical solutions of Schrödinger's equation, resulting in the absence of zero energy states, with all states becoming delocalized throughout the lattice.

Furthermore, by explicitly solving the zero energy eigenstates, it becomes evident that the wave function at the B site within any unit cell will be zero. Conversely, the wave function at the A site will exhibit exponential localization, characterized by a factor of $(\frac{-v}{w})^{x-1}$, where x denotes the unit cell index.

Electrical Circuit Representation of SSH Model

The SSH Hamiltonian of N unit cell is of the form:

$$H = \begin{pmatrix} 0 & v & 0 & 0 & .. \\ v & 0 & w & 0 & ... \\ 0 & w & 0 & v & .. \\ 0 & 0 & v & 0 & w.. \\ 0 & 0 & 0 & .... & 0 \end{pmatrix}_{2N\times 2N}$$

The SSH Hamiltonian can be emulated by a circuit of two repeated circuit elements with different admittances (see figure below) plus two extra grounding elements. It can be described by the circuit's admittance matrix, which can be split into two matrices, one equaling the SSH Hamiltonian and a diagonal matrix scaled with the sum of admittances connected to a unit cell:

$$Y = \begin{pmatrix} Y_1 + Y_2 & -Y_1 & 0 & 0 & .. \\ -Y_1 & Y_1 + Y_2 & -Y_2 & 0 & ... \\ 0 & -Y_2 & Y_1 + Y_2 & -Y_1 & .. \\ 0 & 0 & 0 & .... & Y_1 + Y_2 \end{pmatrix} = \begin{pmatrix} 0 & -Y_1 & 0 & 0 & .. \\ -Y_1 & 0 & -Y_2 & 0 & ... \\ 0 & -Y_2 & 0 & -Y_1 & .. \\ 0 & 0 & 0 & .... & 0 \end{pmatrix} + (Y_1 + Y_2) * I$$

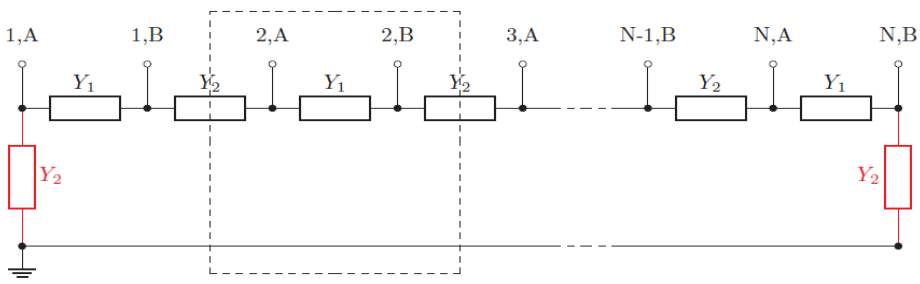

Figure 10: **Schematics of SSH-like circuit with N unit cells containing two sublattice sites A and B. Two red elements make the matrix uniformly diagonal.**[6]

We utilize passive linear components like resistors (R), capacitors (C), and inductors (L) to ensure circuit stability and eliminate voltage-dependent admittances. Within this constraint, we encounter two types of admittances: purely real ($Y_R = 1/R$) for resistors

and purely imaginary ($\mathrm{Y}_C = \mathrm{i}\omega\mathrm{C}$, $\mathrm{Y}_L = \frac{-i}{\omega L}$) for capacitors and inductors, whose values vary with the excitation frequency ω.

In Chapter 2, we established that the eigenvalue spectrum of the SSH chain falls within the range of $\pm(|v|+|w|)$, with topological edge modes emerging when $|v| < |w|$. To manipulate the eigenvalue spectrum around zero admittance, two approaches are considered. One option involves employing distinct frequency-dependent circuit elements to represent various hopping terms. However, this approach presents challenges, as it can't map back to the non-complex SSH model when pairing real and imaginary admittances as hopping elements.

The alternative approach utilizes inductors (L) and capacitors (C) as hopping elements, resulting in purely imaginary eigenvalues. In this combination, the spectral range no longer centres on zero, and its position shifts with frequency. However, as eigenvalues cross zero and dominate the admittance matrix at different frequencies, the ratio between the frequency-dependent hopping elements varies. Consequently, the frequency-dependent nature of these hoppings results in distinct configurations of the SSH model for each dominating eigenvector with an eigenvalue near zero. This dynamic behaviour leads to a rich and frequency-dependent circuit response, where each dominating eigenvector corresponds to a unique SSH model configuration.

The most practical approach involves incorporating suitable grounding elements. By adding the same grounding element to every node, the admittances only contribute to the shifting term of the eigenvalues. Using the same imaginary circuit elements for hoppings also ensures they consistently scale with frequency. As a result, the SSH configuration remains constant across different measurement frequencies, as it primarily depends on the hopping ratio, providing a stable and consistent circuit model for analysis.

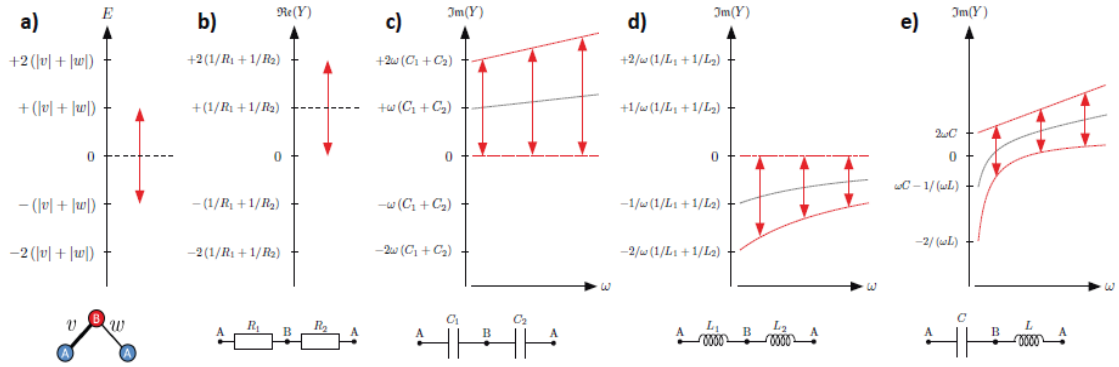

Figure 11: **Eigenvalue ranges of the SSH model and different electric configurations emulating the model. (a)eigenspectrum of SSH model; (b) Positive real spectrum for purely resistive circuit ; (c) Positive imaginary spectrum for purely capacitive circuit; (d) negative imaginary spectrum for purely inductive circuit; (e) eigen spectrum oscillates around zero for LC combined circuit and for higher frequencies, it will be 2ωC, and for lower frequencies, it will be -2/(ωL),** [6]

In considering how to implement the SSH circuit, the choice between resistive and capacitive/inductive hopping and grounding elements plays a critical role. Using resistive hopping elements would necessitate the introduction of variable negative resistances to the ground, which is theoretically achievable with active circuitry. However, this approach requires manual adjustment of the negative resistance to shift the admittance spectrum toward zero, and it can potentially lead to circuit instability due to the energy input by active components. Capacitors and inductors are employed as hopping and grounding elements as a more stable alternative. One type of admittance (either capacitive or inductive) is the hopping element, ensuring a consistent model configuration across all frequencies. The other type of admittance functions as grounding elements, contributing solely to the eigenvalue shift. Importantly, this arrangement guarantees that all eigenvalues pass through zero at a specific finite frequency due to their respective negative admittance compared to the hopping elements. This implementation allows for selective exploration of different eigenstates within the same SSH configuration at various AC frequencies. The frequency-dependent spectrum shifts are illustrated in the above figure. Ultimately, this approach offers stability, controllability, and precision, making it the preferred choice to implement the SSH circuit using capacitive/inductive elements while ensuring the desired dynamic behaviour across different frequency regimes. But because of the higher quality factor and lower tolerance, we choose capacitors as the hopping elements [6].

In the experimental implementation, careful attention should be paid to minimizing unwanted inductive couplings between circuit elements, as these couplings can introduce

varying effects and alter the Hamiltonian model. Magnetization losses become a concern when using inductors containing magnetic materials, such as cores or for magnetic shielding, especially at higher frequencies. Higher capacitances may be required to maintain a manageable working frequency without increasing inductance values excessively, potentially necessitating ceramic materials with higher permittivity. However, capacitors with higher capacitance can introduce higher ohmic losses, impacting the accuracy of the circuit model. Achieving the right balance among component properties, working frequency (limited by measurement devices), and circuit board layout is crucial. Minimizing component tolerances is essential to reduce random deviations from the ideal solid-state model. This allows for more precise characterization while minimizing the impact of non-ideal components on the circuit's behaviour.

Using inductors (L) and capacitors (C) in our circuit, we can find out the grounded Laplacian, which can mimic the SSH Hamiltonian, as detailed in Chapter 3.

3.3 Chapter 3: Study of Simulated Circuit

Simulation using Python

The last section discusses constructing an SSH model using L and C components in the electrical circuit. Let us now consider constructing this SSH model using L and C components. The Hamiltonian of the SSH model is a tridiagonal matrix (see Chapter 2). And the Grounded Laplcain of any circuit is of the form (see Chapter 1)

$$J = D - C + W \tag{23}$$

D and W are always a Diagonal matrix, so the Diagonal entries are unavoidable from the expression of J, but then H (see Chapter 2) has zero diagonal entries. This suggests that our circuit will behave as Topological only in specific regimes; this condition is termed 'Resonance'. By grounding our circuit, we are making our circuit behave as an open boundary SSH chain. Let us write down the J matrix of the circuit (see figure below).

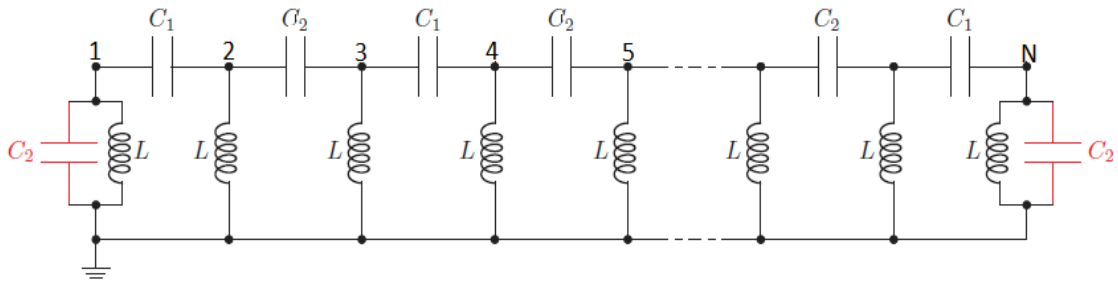

Figure 12: **Topoelectrical circuit for SSH Model**[6]

$$C = i\omega \begin{pmatrix} 0 & C_1 & 0 & 0 & ... & 0 \\ C_1 & 0 & C_2 & 0 & ... & 0 \\ 0 & C_2 & 0 & C_1 & .. & 0 \\ 0 & 0 & C_1 & 0 & ... & 0 \\ 0 & 0 & 0 & 0 & C_1 & 0 \end{pmatrix}_{2N\times 2N} \qquad D = i\omega * Diag\left(C_1, C_1 + C_2, , C_1 + C_2, ..., C_1\right)_{2N\times 2N}$$

$$W = \begin{pmatrix} i\omega C_2 + \frac{1}{i\omega L} & 0 & 0 & 0 & ... & 0 \\ 0 & \frac{1}{i\omega L} & 0 & 0 & ... & 0 \\ 0 & 0 & \frac{1}{i\omega L} & 0 & .. & 0 \\ 0 & 0 & 0 & \frac{1}{i\omega L} & ... & 0 \\ . & . & . & . & & \\ 0 & 0 & 0 & 0 & 0 & \frac{1}{i\omega L} + i\omega C_2 \end{pmatrix}_{2N\times 2N} \tag{24}$$

Therefore, the total conductance of the circuit or grounded circuit Laplacian 'J' will be as follows:

$$J = i\omega \begin{pmatrix} C_1 + C_2 - \frac{1}{w^2 L} & -C_1 & 0 & 0 & ... & 0 \\ -C_1 & \frac{-1}{w^2 L} + C_1 + C_2 & -C_2 & 0 & ... & 0 \\ 0 & -C_2 & \frac{-1}{w^2 L} + C_1 + C_2 & -C_1 & .. & 0 \\ 0 & 0 & -C_1 & \frac{-1}{w^2 L} + C_1 + C_2 & ... & 0 \\ . & . & . & . & & \\ 0 & 0 & 0 & 0 & 0 & C_1 + C_2 - \frac{1}{w^2 L} \end{pmatrix}$$

For this configuration, the diagonal entries in J are symmetrical, and this circuit Laplacian will behave as an SSH Hamiltonian when we make the diagonal entities of the J to be zero or drive the circuit at the resonant frequency given by

$$w_r = \frac{1}{\sqrt{L(C_1 + C_2)}} \tag{25}$$

To understand the topological phase of an electrical circuit, we can measure impedance between two points. The impedance depends on the eigenvalues of the matrix J, which resembles the SSH Hamiltonian. We observe a sharp peak at the resonance frequency in the topological phase with zero energy states in the impedance measurement. Conversely, in the trivial phase without zero energy states, we do not observe any sharp peaks in the impedance at resonance frequency, providing a clear distinction between the two phases. Also, we may get some additional peaks, other than resonance frequencies for both the topological and trivial phase; those peaks don't signify anything, as the grounded Laplacian (L) mimics the SSH Hamiltonian only at the resonance frequency.

As discussed in Chapter 1, the impedance between any two nodes can be measured by finding eigenvalues and eigenvectors of the J matrix. Using the same principle, we construct a 5-unit cell SSH circuit and find the Impedance between N = 1 and N = 10 nodes for different values of hopping parameter t (here v).

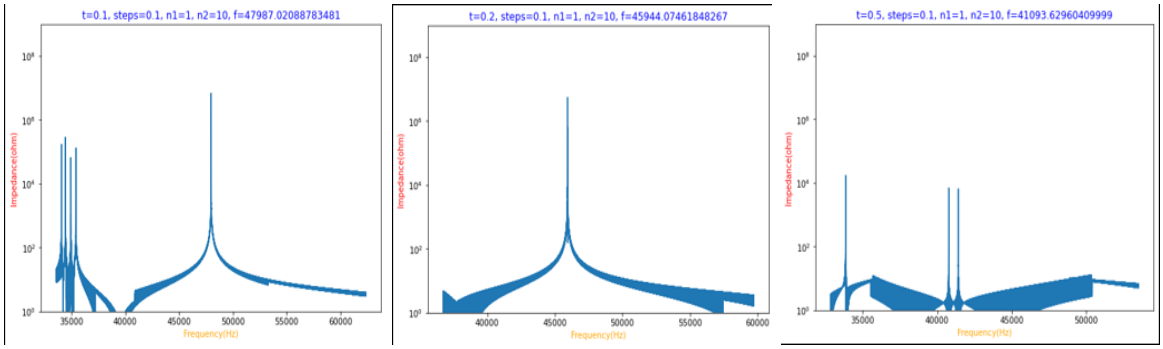

Figure 13: **Impedance of the circuit for v(=t)** < 1

In the regime where $v < 1$, a sharp resonance peak, accompanied by secondary peaks at different frequencies, is observed. This resonance phenomenon aligns with zero eigenmodes, as we can anticipate a sharp peak precisely at the frequency corresponding to a zero eigenvalue of the grounded Laplacian. In the case of the topological configuration, where a zero or near-zero eigenvalue is present, it manifests as the peak in the impedance spectrum, confirming the association between zero eigenmodes and the resonance behaviour observed in the impedance measurements.

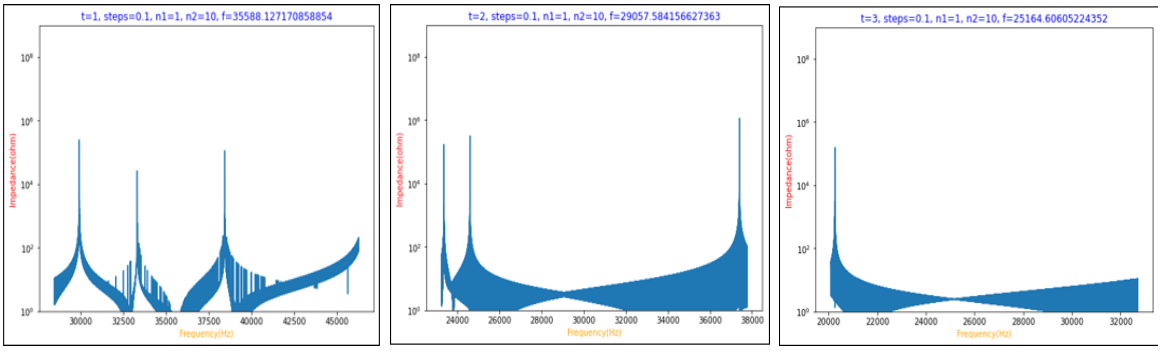

Figure 14: **Impedance of the circuit for v** > 1

Now, for the v < 1 case, we get that the impedance has no sharp peak at f $=$ f$_r$, which depicts the trivial phase of the circuit.

It's important to note that secondary peaks occur in both topological and trivial cases. Therefore, the key distinguishing factor lies in the presence of the peak at the resonance frequency. To ensure accuracy while handling the computational aspects, we've chosen a step size of 0.1. While this step size is sufficient for computer-based calculations, further accuracy can be achieved by reducing it, perhaps with the aid of a cluster or supercomputer. However, it's worth emphasizing that the results obtained thus far are already effective in distinguishing between the topological and trivial behaviours of the circuit.

Simulation using LT spice

We used LT Spice Software to measure impedance in the circuit more realistically. It allows us to build virtual circuits and characterize them using various tools available in the software. We constructed topological and trivial circuits for N = 10 and N = 5 unit cells with L = 10uH, C_1 = 0.1uF and C_2 = 0.22uF.

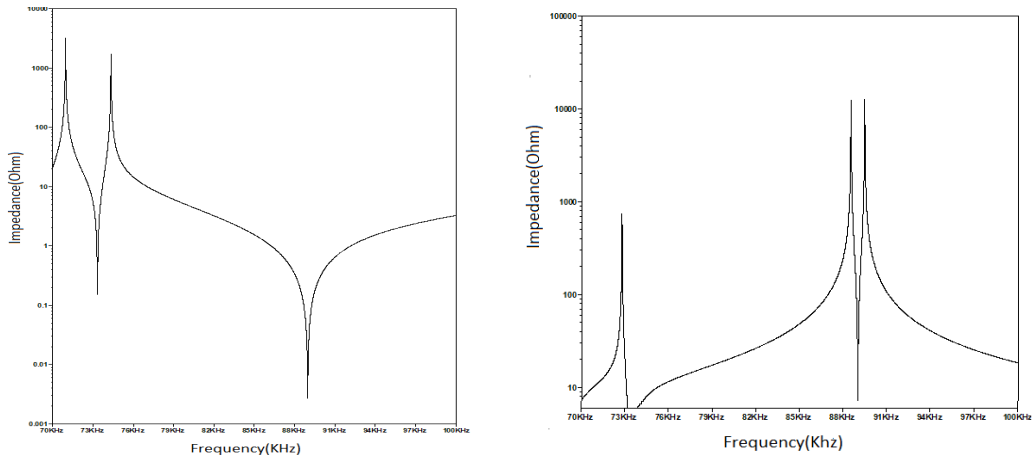

Figure 15: Trivial & Topological for N = 5 unit cells

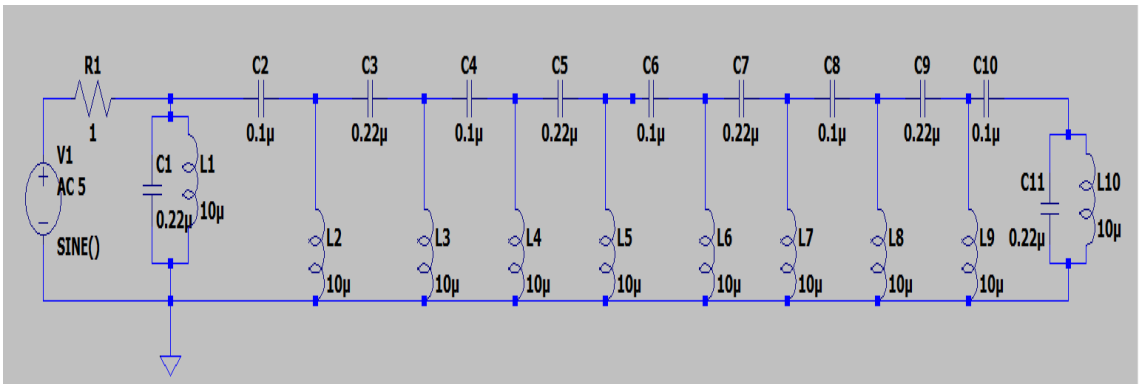

Figure 16: Topological Circuit for N = 5 unit cells

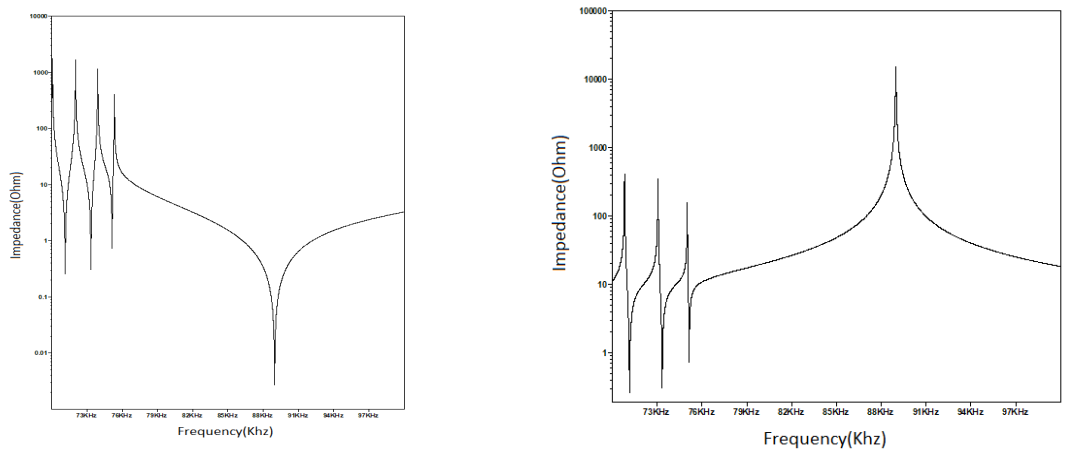

Figure 17: Trivial & Topological for N = 10 unit cells

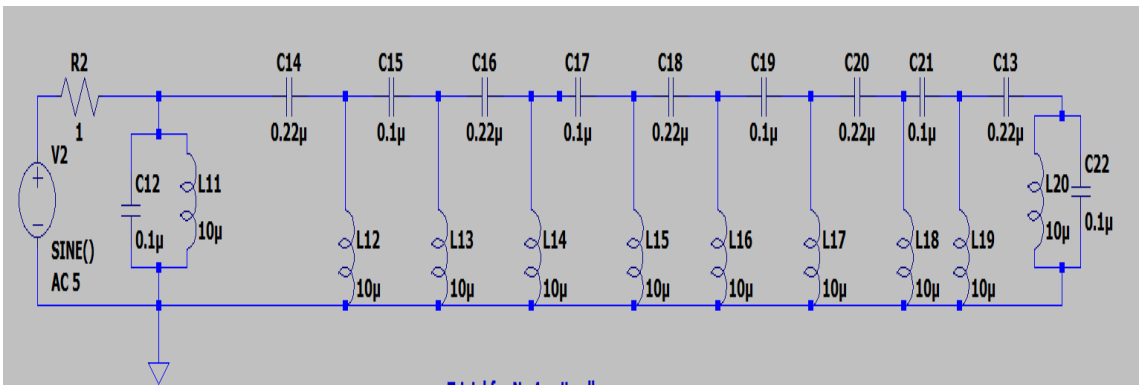

Figure 18: Trivial Circuit for N = 5 unit cells

For the case of an N=5 unit cell, the topological phase is not clear, and there is an unexpected drastic decrease in impedance near resonant frequency (88.97 KHz). The reason is that for the small chain, the smaller eigenvalue of the Laplacian is larger than that of the bigger chain. Hence, we think this experiment should be carried out with a larger number of lattices and a minimum of 10 to observe a good response.

Let us discuss one important point regarding the Impedance measurement. Measuring the impedance between any two nodes in the middle of the circuit(bulk) is challenging. Probing using lock-in techniques or an oscilloscope might not be possible, although this can be done theoretically. In measuring the impedance between two points, voltage difference can be measured. Still, the current can't be measured since the source is connected at the edge, which limits us from doing any analysis to calculate the effective impedance between the two points. However, using Python, we plotted impedance measured between N =1 cell and N = 5 cell (see previous section). Experimentally, we can probe the leftmost edge easily since the circuit simplifies.

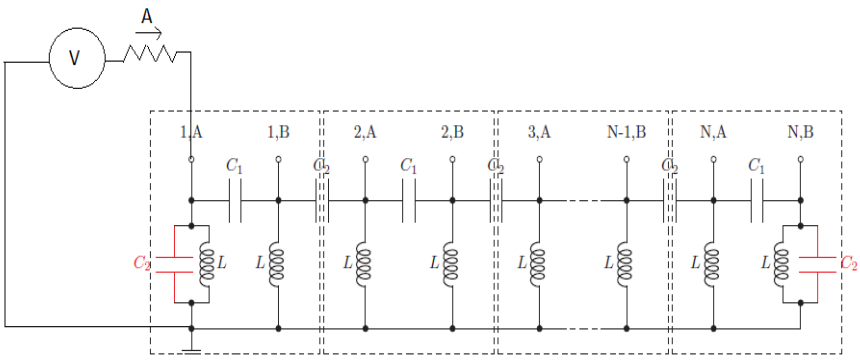

Figure 19: **Impedance measurement between 1A node and Ground**

Measuring impedance at the leftmost edge has the advantage that the circuit(fig-15) can be transformed into a simpler one fig(16). Impedance can be measured by measuring current using a shunt resistance and potential difference between two nodes. This effectively gives the impedance of the whole circuit.

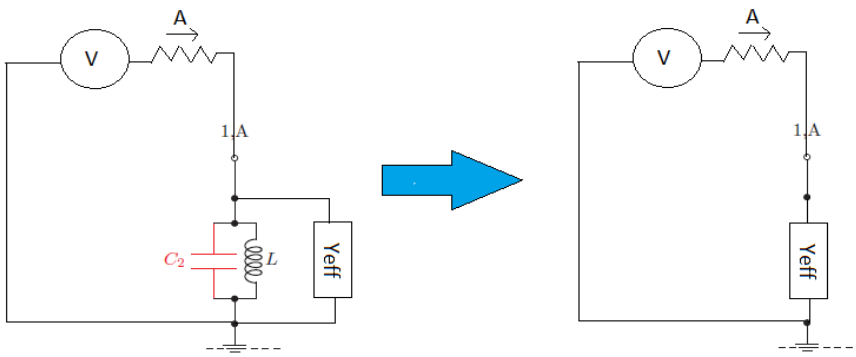

Figure 20: **Impedance measurement at leftmost edge**

We introduce a small shunt resistance in the circuit to measure the current. This resistance doesn't affect our grounded Laplacian, so it mimics the SSH Hamiltonian at resonance frequency. Therefore, this resistance has no role in the circuit except it can only help us the current across the Y_{eff}.

3.4 Chapter 4: Experimental Implementation

Brief on Lock In Amplifier

Lock-in amplifiers are used to detect and measure very small AC signals - all the way down to a few nanovolts. Accurate measurements may be made even when the small signal is obscured by noise sources many thousands of times larger. Lock-in amplifiers use a technique known as phase-sensitive detection to single out the component of the signal at a specific reference frequency and phase. Noise signals, at frequencies other than the reference frequency, are rejected and do not affect the measurement.

Let us briefly discuss the Phase sensitive detection. Lock-in measurements require a frequency reference. Typically, an experiment is excited at a fixed frequency (from an oscillator or function generator), and the lock-in detects the response from the experiment at the reference frequency. If the sine output from the function generator is used to excite the experiment, the signal is $V_0 Sin(\omega_s t + \theta_{sig})$, where V_0 is the signal amplitude, ω_s is the signal frequency, and θ_{sig} is the signal's phase. Now, if the external reference can be provided externally or internally [8] of the form $V_r Sin(\omega_r t + \theta_{ref})$, then the PSD (phase sensitive detector) will multiply the signal & reference and generate two signal with different frequency component. Therefore, the output of the PSD is simply the product of two sine waves.

$$V_{psd} = V_0 V_r Sin(\omega_s t + \theta_{sig}) Sin(\omega_r t + \theta_{ref})$$
$$= \frac{V_0 V_r \cos([\omega_s - \omega_r]t + [\theta_{sig} - \theta_{ref}])}{2} - \frac{V_0 V_r \cos([\omega_s + \omega_r]t + [\theta_{sig} + \theta_{ref}])}{2} \quad (26)$$

The PSD output is two AC signals, one at the difference frequency (ω_s - ω_{ref}) and the other at the sum frequency (ω_s + ω_{ref}). The AC signals are removed if the PSD output is passed through a low-pass filter. And if $\omega_s = \omega_{ref}$, the difference in frequency of the component will be a DC signal. In this case, the filtered PSD the output will be:

$$V_{psd} = \frac{V_0 V_r \cos(\theta_{sig} - \theta_{ref})}{2} \quad (27)$$

This is a very nice signal DC signal proportional to the signal amplitude.

We got that the PSD output is proportional to $V_0 \cos\theta$, where $\theta = \theta_{sig} - \theta_{ref})$ is the phase difference between the signal and the lock-in reference oscillator. By adjusting θ_{sig}, we can make θ equal zero. In this case, we can measure $V_0(cos\theta = 1)$. Conversely, there will be no output if θ is $90^0(cos\theta = 0)$.

This phase dependency is a little problematic, which can be eliminated by adding a second PSD. If the second PSD multiplies the signal with the reference oscillator shifted by 90^0,

i.e. $V_r Sin(\omega_r t + \theta_{ref})$, its low pass filtered output will be:

$$V_{psd} = \frac{V_0 V_r \sin(\theta_{sig} - \theta_{ref})}{2} \tag{28}$$

Now, we have two outputs: one proportional to $\cos\theta$ and the other proportional to $\sin\theta$. If we call the first output X and the second Y, X $\sim V_0 \cos\theta$, Y $\sim V_0 \sin\theta$, these two quantities represent the signal as a vector relative to the lock-in reference oscillator. X is called the 'in-phase' component, and Y is the 'quadrature' component. This is because when $\theta = 0$, X measures the signal while Y is zero. The phase dependency is removed by computing the signal vector's magnitude R, where R $\sim \sqrt{X^2 + Y^2} = \mathrm{V}_0$. Therefore, R measures the signal amplitude and does not depend upon the phase between the signal and lock-in reference. A dual-phase lock-in has two PSDs (e.g, 'MoKu: Go') with reference oscillators 90^0 apart and can directly measure X, Y and R. In addition, the phase (θ) between the signal and lock-in is defined as: $\theta = \tan^{-1}(\mathrm{Y/X})$

Figure 21: **'Mocu: Go' Lock-in-amplifer**

We employed the "Mocu: Go" lock-in amplifier (see figure above) for our measurements to gauge the impedance by capturing the voltage across the circuit. Given the relatively low voltage levels involved, we opted for the precision of the "Mocu: Go" instead of an oscilloscope, which could also be used for voltage measurements [9].

Impedance Profile

Chapter 1 delves into the analytical measurement of impedance between any two nodes. In our SSH model, a noteworthy zero energy state, also known as a mid-gap state, emerges in the scenario of a finite chain or open boundary condition (OBC) case, as elucidated in Chapter 2. This occurrence is prevalent when the system resides in a topological state (i.e. when v < w). The presence of this mid-gap state results in a distinctive peak in the impedance vs frequency curve during resonance for the topological case. In contrast, the trivial case lacks a sharply defined peak under similar conditions.

Chapter 3 focuses on the systematic circuit impedance measurement. The methodology

involves measuring the root mean square voltage (V_{rms}) across the circuit and introducing a shunt resistance (with a value of 1Ω). Since the shunt resistance is purely resistive, it does not impact the phase relationship between current (I) and voltage (V). The root mean square current (I_{rms}) is obtained by dividing the measured voltage by the resistance value. Ultimately, the impedance of the circuit is determined by dividing V_{rms} by I_{rms}.

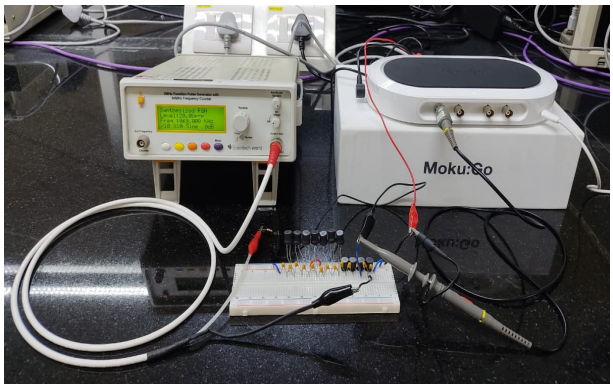

Figure 22: **Experimental Set up**

As depicted in the provided figure, we implemented our circuit for 6 unit cells on a breadboard. An input signal is generated using a frequency generator, and the resulting output signal is measured using the "Mocu: Go" lock-in amplifier. To effectively distinguish between the topological and trivial phases, data is systematically gathered by sweeping the frequency within a range spanning from 60 kHz to 150 kHz with a step of 1 kHz. This frequency span is selected based on the theoretically calculated resonance frequency, which hovers around 89 kHz. The frequency variation facilitates the acquisition of data that accentuates the distinct characteristics of the topological and trivial phases. Below, the impedance graph illustrating the differences in these phases is presented.

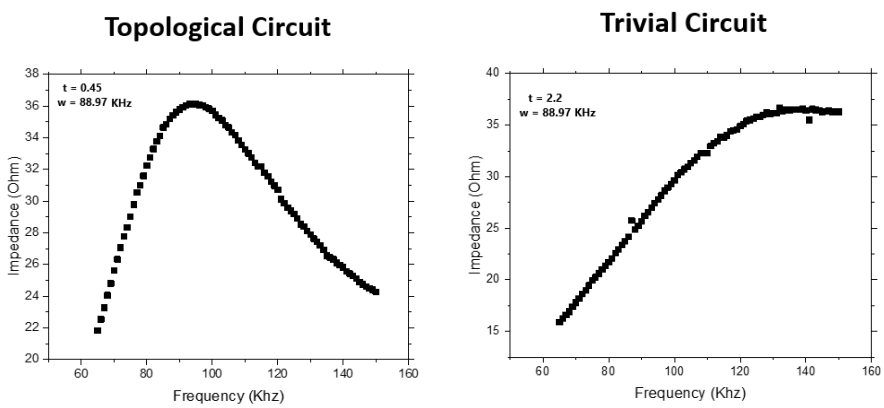

Figure 23: **Impedance profile of Topological and Trivial Phase**

4 Result and Analysis

Chapter 4's impedance profile analysis reveals a distinct disparity between the topological and trivial phases. In the topological scenario, a sharp peak emerges in correspondence to the mid-gap state during resonance. This peak serves as a signature feature indicative of the topological phase. Conversely, such a mid-gap state is absent in the trivial case, leading to a notably different impedance profile. While the impedance in the trivial case consistently increases with frequency, it reaches saturation after 130 kHz. This saturation effect serves as an additional distinguishing characteristic between the two phases. Furthermore, the decision to collect data at a 1 kHz frequency step provides a broad overview, but it is noted that refining the data collection with smaller frequency steps could potentially yield more granular and nuanced insights into the impedance behaviour, especially in regions of interest such as around resonance.

The construction of our circuit on the breadboard introduces a challenge related to the contact resistance, leading to a slightly elevated impedance in the trivial phase. The contact resistance, inherent in the breadboard setup, contributes to this deviation from the expected impedance values. Additionally, utilising inductors with substantial internal resistance affects the resonance peak in the topological case. The internal resistance of the inductors introduces a broadening effect on the peak at resonance, influencing the sharpness and clarity of the mid-gap state signature.

5 Conclusion

This project encompassed a thorough exploration of the SSH model, employing a dual approach involving both simulation and experimental methodologies. A substantial portion of our efforts focused on validating the Laplacian formalism, which facilitated the mapping of tight-binding Hamiltonian properties onto an electric circuit. Notably, we leveraged simulation-based impedance measurements to initially indicate the presence of eigenstates with eigenvalues close to zero. This was complemented by experimental impedance versus frequency measurements, allowing for a detailed examination of the mid-gap state and the differentiation of two distinct phases of matter: the topological and trivial.

Our results yielded positive outcomes, aligning well with theoretical expectations in both simulation and experimentation. A meticulous exploration of the topological phase included a compelling impedance comparison between the topological and trivial circuit configurations. While direct verification of boundary localization through experimentation proved challenging, our impedance data provided valuable insights into the circuit's behaviour across topological and trivial phases.

Despite encountering some experimental challenges, we can confidently assert the overall success of this project. The integration of simulation and experimental data significantly advanced our understanding of the SSH model and underscored the validation of the Laplacian formalism within electric circuits.

6 Future Plans

This project has given us a valuable introduction to this emerging and captivating research field. Despite encountering experimental challenges and facing limitations in terms of available components, our aspirations for the project are structured as follows:

1. Validate the localization of boundary modes by measuring the voltage at different nodes at the edges by employing high-quality capacitors and inductors.

2. Undertake the construction and study of higher-dimensional topological insulators to better understand the higher-dimensional objects.

3. Engage in the simulation of other tight-binding models to comprehensively explore the diverse physical phenomena that can arise in condensed matter systems.

These outlined plans represent our vision for future endeavors, aiming to expand our understanding of topolectrical physics by addressing experimental constraints and exploring diverse aspects of the field.

Acknowledgement

I extend my heartfelt gratitude to my course instructor, Dr. Kartikeswar Senapathi, as well as to Dr. Tapan Mishra and Dr. Saralasrita Mohanty, for their invaluable guidance and for illuminating my path into the fascinating field of topolectrical physics. I sincerely thank Dr. Gunda Santosh Babu for his steadfast support within the laboratory throughout the project. Their collective expertise and unwavering guidance have enhanced my understanding and learning experience in this complex field.

I must acknowledge my dedicated lab partner, Shubhay Dikkar, for his indispensable assistance conducting experiments and engaging in enlightening project-related discussions. Additionally, I would like to thank Soumya Ranjan Padhi Bhaiya for his wholehearted encouragement and technical guidance.

In my quest to understand Topological Physics, I am indebted to the invaluable resources provided by Asboth's book and Gautam Sheet's paper on Topological Insulators. These texts were my primary sources for a deeper comprehension of the subject. Furthermore, I thank Dr. Andrew Mitchell for his outstanding lecture on "Topological Quantum Matter."

Last but certainly not least, I want to extend my heartfelt thanks to my friends, fellow lab students, and all those who provided mental and physical support throughout this project. Their contributions have been the cornerstone of my strength during this endeavour. I am humbled and privileged to have been surrounded by such remarkable individuals and resources. Words alone cannot adequately express my gratitude for their unwavering support.

7 References

1. F Y Wu, *Theory of resistor networks: the two-point resistance, J. Phys. A: Math. Gen. 37 (2004) 6653–6673*

2. Navketan Batra & Goutam Sheet, *Understanding Basic Concepts of Topological Insulators Through Su-Schrieffer-Heeger (SSH) Model, arXiv:1906.08435, 2019*

3. W. P. Su, J. R. Schrieffer, & A. J. Heeger, *Solitons in Polyaeetylene, Physical Review Letters, Volume 42, Number 25*

4. J. K. Asboth, L. Oroszlany and A. Palyi, *A Short Course on Topological Insulators, arXiv:1509.02295, 2015*

5. Ching Hua Lee, Stefan Imhof, Christian Berger, Florian Bayer, Johannes Brehm, Laurens W. Molenkamp, Tobias Kiessling & Ronny Thomale, *Topolectrical Circuits, Communications Physics volume 1, Article number: 39 (2018)*

6. Stefan Michael Imhof, *The effects of non-Hermiticity and non-linearity on topological phenomena investigated in electric networks, PhD dissertation, 2023*

7. David Tong, *Quantum Hall Effect, Lecture Notes, 2016*

8. Standford Research System, *About Lock-In Amplifiers*, User Manual

9. Russell Yang Qi Xun, *Topological Circuits - A Stepping Stone in the Topological Revolution*, Mol.Front. J, 2020